

# The influence of nucleation on the spectral content of cloud cavitation about a hydrofoil

<sup>1</sup>James Venning\*; <sup>1</sup>Dean Giosio; <sup>1</sup>Samuel Smith; <sup>1</sup>Bryce Pearce; <sup>1</sup>Paul Brandner;

<sup>1</sup>*Cavitation Research Laboratory, Australian Maritime College, University of Tasmania, Australia;*

## Abstract

The influence of nucleation on the spectral content of cloud cavitation is investigated using unsteady force measurements and simultaneous high-speed imaging of a rectangular planform NACA-0015 section hydrofoil, with and without upstream nuclei injection. Experiments were conducted for cavitation numbers over the range of 0.60 to 0.45, at a chord-based test Reynolds number of  $1.4 \times 10^6$ , and at an incidence of  $6^\circ$ . The introduction of freestream nuclei was found to significantly alter the cavity topology and spectral content of the force response. Three shedding modes were observed in the case without nuclei injection, while two modes were present with the injection of abundant freestream nuclei. In the nuclei deplete case the dominant shedding frequency is associated with upstream shock propagation and was found to decrease with test cavitation number from a Strouhal number of 0.311 to 0.243, while the sub-harmonic and first harmonic were associated with localized tip and root activity. With the introduction of nuclei the dominant of two distinct shedding frequencies was found to be the lower frequency mode at approximately half that of the corresponding nuclei deplete case, with Strouhal number decreasing from 0.159 to 0.148. The higher frequency mode was shown to be due the propagation of an initial shockwave that only partially condenses the cavity prior to the passage of a second shockwave that leads to full span-wise condensation.

**Keywords:** cavitation; nucleation; spectral content; cavity dynamics

## Introduction

The formation, separation and collapse of sheet cavities (i.e. partial cavitation) is generally described as cloud cavitation. For sufficiently thick cavities the re-entrant jet, associated with the cavity closure, has sufficient intensity to propagate upstream and penetrate the cavity interface causing a portion of the cavity to detach. This detached cavity undergoes condensation, resulting in a bubbly cloud that is then advected away by the bulk flow. This phenomenon has been widely studied, both experimentally and numerically, in various contexts including hydrofoils [1-3], rotating machinery [4], nozzles/venturies [5], wall-mounted cavitators [6] and bluff bodies [7, 8]. Recently it has been shown that the formation of condensation shockwaves produce another shedding mechanism, either independently or coupled with a re-entrant jet, leading to cavity de-stabilisation [9, 10]. Three-dimensional flow features have been shown to significantly alter the re-entrant flow behaviour and the resulting shedding physics [11], as was also observed in the present study. The inception of hydrodynamic cavitation in practical flows is invariably due to heterogeneous nucleation. These discrete sites of weakness, termed nuclei, are typically either free microbubbles within the liquid volume, or volumes of gas trapped in or on adjacent surfaces. Nuclei have been shown to control not only inception [12] but also the dynamics of cavitation [13]. In the current work the effect of nuclei injection and cavitation number on the spectral content of a cavitating finite span hydrofoil is presented.

## Experimental Overview

Experiments were performed in the variable pressure Cavitation Research Laboratory (CRL) water tunnel at the Australian Maritime College (AMC). The 365 m<sup>3</sup> capacity tunnel (demineralized water, conductivity of order 1 $\mu$ S/cm) is fitted with ancillary systems for strict control of dissolved oxygen content and continuous removal of nuclei and incondensable gas volumes. The free stream velocity and operating pressure in the 0.6 m square test section can be independently controlled within the ranges of 2 to 12 ms<sup>-1</sup> and 4 to 400 kPa absolute, respectively. The test section velocity is spatially uniform to within  $\pm 0.5\%$ , with temporal variations of less than 0.2%, while the free stream turbulent intensity is approximately 0.5%. Upstream of the test section a geometrically configurable array of microbubble generating devices allow for controlled nuclei injection. A schematic of the experimental facility is given in Figure 1, while a more detailed description of the facility is given in [14].

\*Corresponding Author, James Venning: [James.Venning@utas.edu.au](mailto:James.Venning@utas.edu.au)

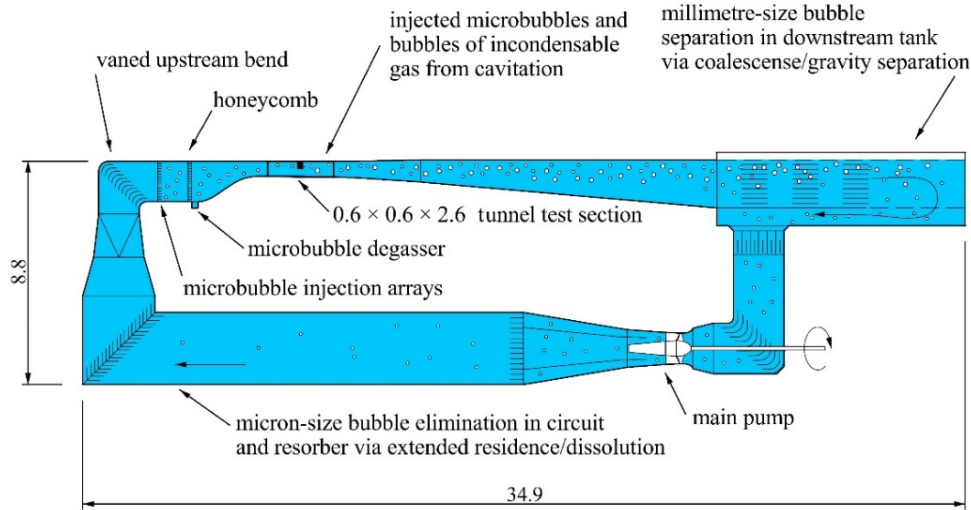


Figure 1: Schematic of the CRL water tunnel circuit. The facility is designed for continuous injection and separation of incondensable gas and cavitation nuclei via processes of coalescence/gravity separation of bubbles greater than about 100  $\mu\text{m}$  in a downstream tank and dissolution of smaller sized bubbles via extended residence in the lower limb, or resorber. All dimensions are given in metres.

An anodized aluminium NACA-0015 section hydrofoil was vertically mounted in the centre of the test section ceiling on a 6-component force balance for acquisition of dynamic force data. The rectangular planform hydrofoil had a chord length,  $c$ , of 0.15 m and a span-wise dimension,  $s$ , of 0.30 m with a faired tip.

Measurements were made at a chord-based Reynolds number of  $1.4 \times 10^6$  over a range of cavitation numbers from 0.45 to 0.60 with the hydrofoil at a fixed incidence of  $6^\circ$ . The Reynolds number is defined as  $Re = U_0 c / \nu$ , where  $U_0$  is the test section velocity,  $c$  is the chord, and  $\nu$  is the kinematic viscosity of water; the cavitation number is defined as  $\sigma = (p_0 - p_v) / \frac{1}{2} \rho U_0^2$ , where  $p_0$  is the static pressure at the hydrofoil tip (test section centerline),  $p_v$  is the vapour pressure, and  $\rho$  is the water density. Simultaneous measurements of hydrofoil normal force and high-speed photography of the cavitation were acquired at 7 kHz for a period of 3 s at each test condition for investigating the phasing of the shedding mechanism. High-speed images were acquired using a LaVision HighSpeedStar8 12-bit camera at a resolution of 1024 x 1024 pixels with a Nikkor f/1.4 50 mm lens. Additional force data for obtaining high-resolution spectra were recorded at 1 kHz for 240 s giving about 5,000 cycles of the dominant frequency. The Power Spectral Density (PSD) were derived using the Welch estimate with a window size of 4096 points (4.1 s) and overlap of 256 points (0.26 s).

Two conditions were investigated where the freestream is either deplete of nuclei, or with abundant injected nuclei, at a dissolved oxygen content of  $\sim 3$  ppm for both cases. The nuclei deplete case is devoid of any active nuclei [15] while for the abundant case homogeneous nuclei injection was achieved using a  $3 \times 10$  array of poly-disperse microbubble generators producing a dominant size of 10 to 15  $\mu\text{m}$  at a concentration of  $\sim 100 \text{ cm}^3$  [16].

## Results

For all cases the cavity shedding was found to be highly periodic as shown in the PSD of the hydrofoil body-normal force, presented below in Figure 2. Continuous wavelet transforms of force data (not presented here) were performed to discriminate between and identify those peak frequencies associated with the cavitating flow physics from those being artefacts of the PSD processing. Additionally, fast Fourier transform (FFT) analysis of pixel intensities from the high-speed photography was undertaken to highlight regions of maximum variation, or energy, within the flow. Amplitudes of the identified peak frequencies are presented in Figure 3 to assist in visualising the shedding mechanisms associated with each frequency, while space-time plots at various hydrofoil locations are presented later in Figure 4.

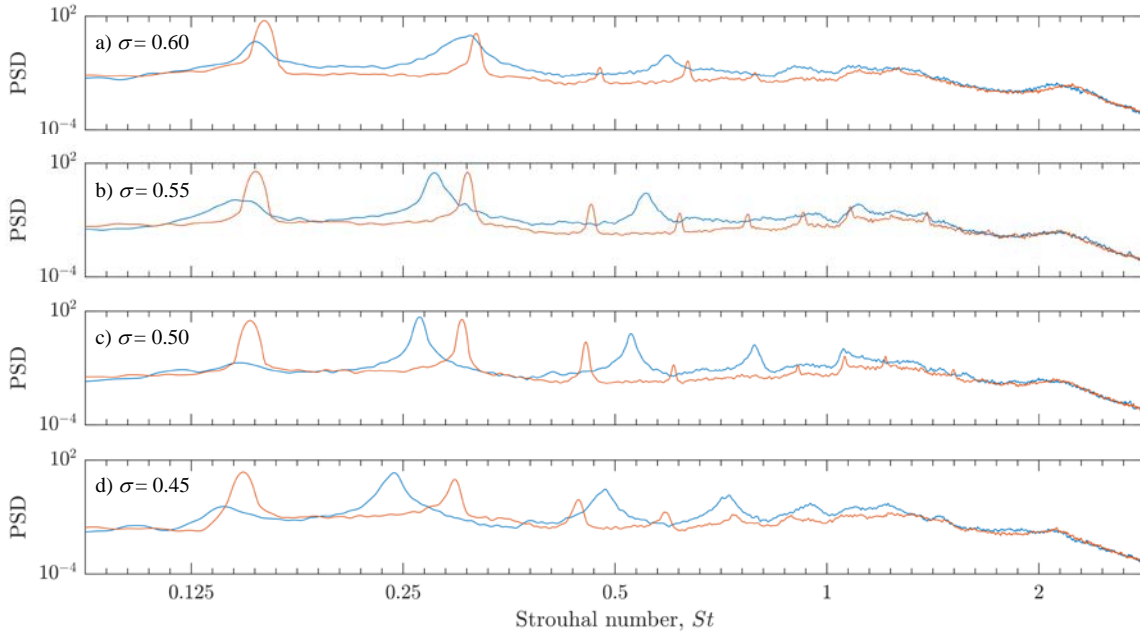


Figure 2: Comparison of the hydrofoil body-normal force spectra with abundant nuclei injection (red), and deplete of nuclei (blue).

For the nuclei deplete case three peak frequencies were observed over the range of tested  $\sigma$  values,  $0.60 \geq \sigma \geq 0.45$ , the dominant frequency decreasing with cavitation number from a Strouhal number,  $St = fc/U$ , of 0.311 to 0.243 (Figure 2(a) – (d)), where  $f$  is the shedding frequency. Visual examination and FFT analysis of the high-speed imaging reveals this dominant frequency to be associated with large-scale cavity growth and subsequent condensation/collapse occurring over a significant portion of the hydrofoil. This is evident in Figure 3(c) showing a reconstruction of the image frame at  $\sigma = 0.55$  expressed as the FFT amplitude of each pixel a Strouhal number of 0.277. The high amplitude region is seen to extend over a distance of approximately  $0.5s$ , centred at  $\sim 0.35s$ . The first frequency peak, occurring at half the dominant frequency for all  $\sigma$  values, is associated with local cavity shedding near the hydrofoil tip (Figure 3(b)) such that there are two distinct, but coupled shedding regions, while the third peak at around twice the main shedding frequency is associated with both tip and root activity (Figure 3(d)). This spectral behavior is further illustrated in the space-time plots given in Figure 4. By inspection of the force time-series, and analysis of the space-time plots, it was shown that the relative strength between the first harmonic and the sub-harmonic shedding mode tended to alternate irregularly. Furthermore, it can be seen from the PSD data that the sub-harmonic peak becomes a minimum at  $\sigma = 0.50$  while, conversely, the higher frequency peak reaches its maximum at this condition.

The large-scale shedding occurs over the mid-half to two-thirds of the span as it is only in this region that the cavity undergoes full chord-wise collapse. As such, during the growth phase the cavity exhibits a crescent-shaped closure region as the cavity regrows from the hydrofoil leading edge at mid-span (Figure 3(a)). A re-entrant jet is formed, the upstream extent of which remains almost stationary as the growing cavity reaches the hydrofoil trailing edge. Although the re-entrant jet may occasionally break through the surface of the growing cavity it does not initiate a shockwave as has been observed for flows about bodies with much greater adverse pressure gradients [10]. As the cavity reaches the trailing edge region shockwaves are triggered, initially at the root and tip which then propagate and focus at the mid-span, leading to the condensation of the cavity in this region as the wave travels upstream and the cycle begins anew.

For the nuclei abundant case the shedding physics are altered due to the high concentration of continuously activated nuclei. The fundamental frequency of the bulk shedding is at  $St \approx 0.15$  corresponding in this case to the first peak in the force PSD (Figure 3) and shows only a slight decrease with cavitation number. This primary shedding is approximately two-dimensional, occurring over the full hydrofoil span (Figure 3(f)).

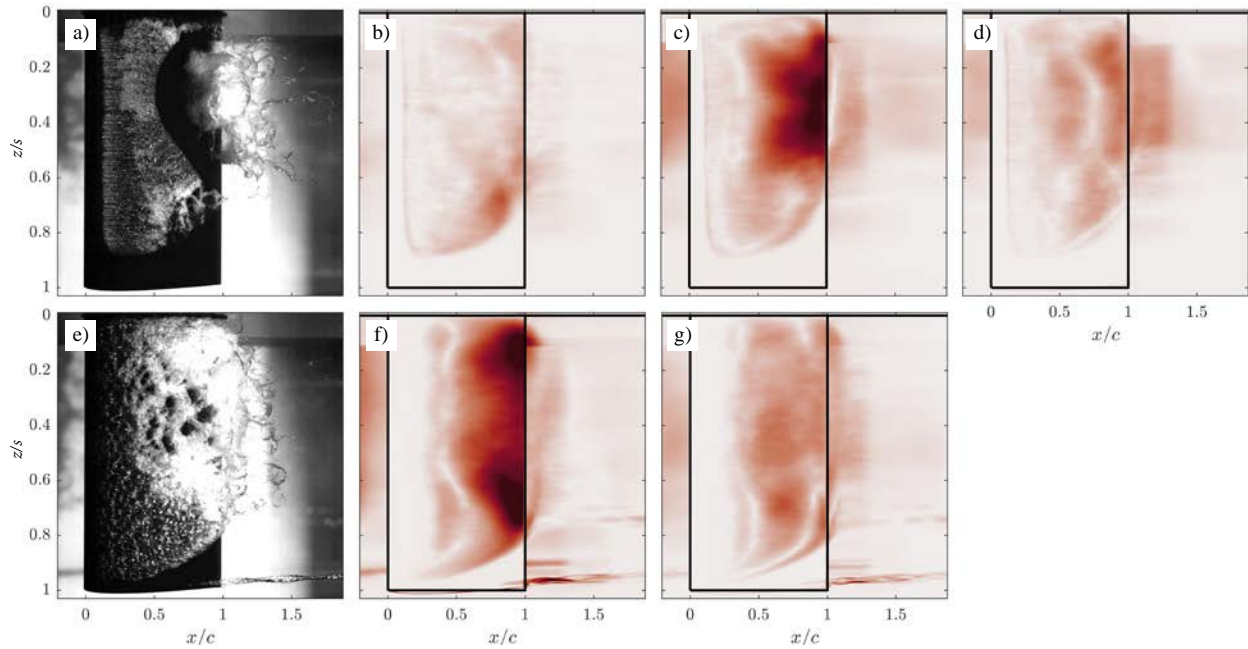


Figure 3: Photographs of the NACA-0015 hydrofoil (a) without, and (e) with nuclei injection, showing the alteration of cavity topology with the addition of nuclei. FFT analysis of pixel intensity from high-speed images are presented for peak frequencies without (top row) and with nuclei injection (bottom row), where (b)  $St = 0.144$ , (c)  $St = 0.277$ , (d)  $St = 0.553$ , (f)  $St = 0.155$ , and (g)  $St = 0.308$ . Both images and FFT analysis are taken at a test condition of  $Re = 1.4 \times 10^6$  and  $\sigma = 0.55$ .

The second peak in the nuclei abundant cases is consistently twice that of the fundamental and can be shown to be associated with the propagation of the first of two shockwaves each cycle. The first shockwave forms once the growing cavity reaches the trailing edge. This shockwave propagates upstream but loses strength and speed, stalling before reaching the cavity leading edge resulting in small-scale localized shedding and condensation. Shortly after this another shockwave forms that travels upstream with greater strength causing large scale condensation with subsequent near- two-dimensional re-growth along the hydrofoil span [17]. Due to the continuous supply of activated nuclei there is no clear cavity detachment line but a discontinuous cavity leading edge such that the cavity is not condensed completely each shedding cycle as was the case for the nuclei deplete case. Nuclei activated at the hydrofoil leading edge grow as they are advected downstream merging to form a contiguous cavity volume. During the growth phase, advected bubbles reach the cavity trailing edge and condense simultaneous with the formation of re-entrant flow. Cavity growth is due to the volume of activated nuclei being greater than the condensing volume at the cavity trailing edge. As described above, once the slow growing cavity reaches the trailing edge, the first shockwave is initiated. As with the nuclei-deplete case the re-entrant jet apparently has no direct influence on the shedding. The peaks at higher frequencies can be shown to be harmonic artefacts of the FFT process.

The space-time plots presented below provide further evidence of the multi-modal nature of the shedding in both nuclei deplete (Figure 4), and nuclei abundant cases (Figure 5). Figure 4(a) presents an ensemble of a single column of pixels extracted from sequential image frames across the length of the span near the trailing edge ( $0.8c$ ), while Figures 4(b) & 4(c) are chord-wise extractions taken at  $0.4s$  and  $0.7s$ , respectively. The large-scale shedding is clearly identified in Figure 4(a) with a cycle composing of the growth phase with re-entrant jet flow, cavity (high intensity pixels) and the passage of a dark vertical band indicating the absence of a cavity. The tip shedding that occurs every alternate cycle is indicated in Figure 4(a) & 4(c), while the consequent alternating strength of the large-scale shedding, initiated at the trailing edge, is evident in Figure 4(b) as shown by the increased speed (solid line) of the shock travelling towards the leading edge following a tip shedding event (as compared with the dashed line).

The two-dimensional nature of the full-span shedding with injected nuclei is evident in the span-wise space-time plot given in Figure 5(a), while the higher frequency small-scale shedding can be seen at mid-span in Figure 5(a) and by the short upstream travelling shock-front indicated in Figure 5(b).

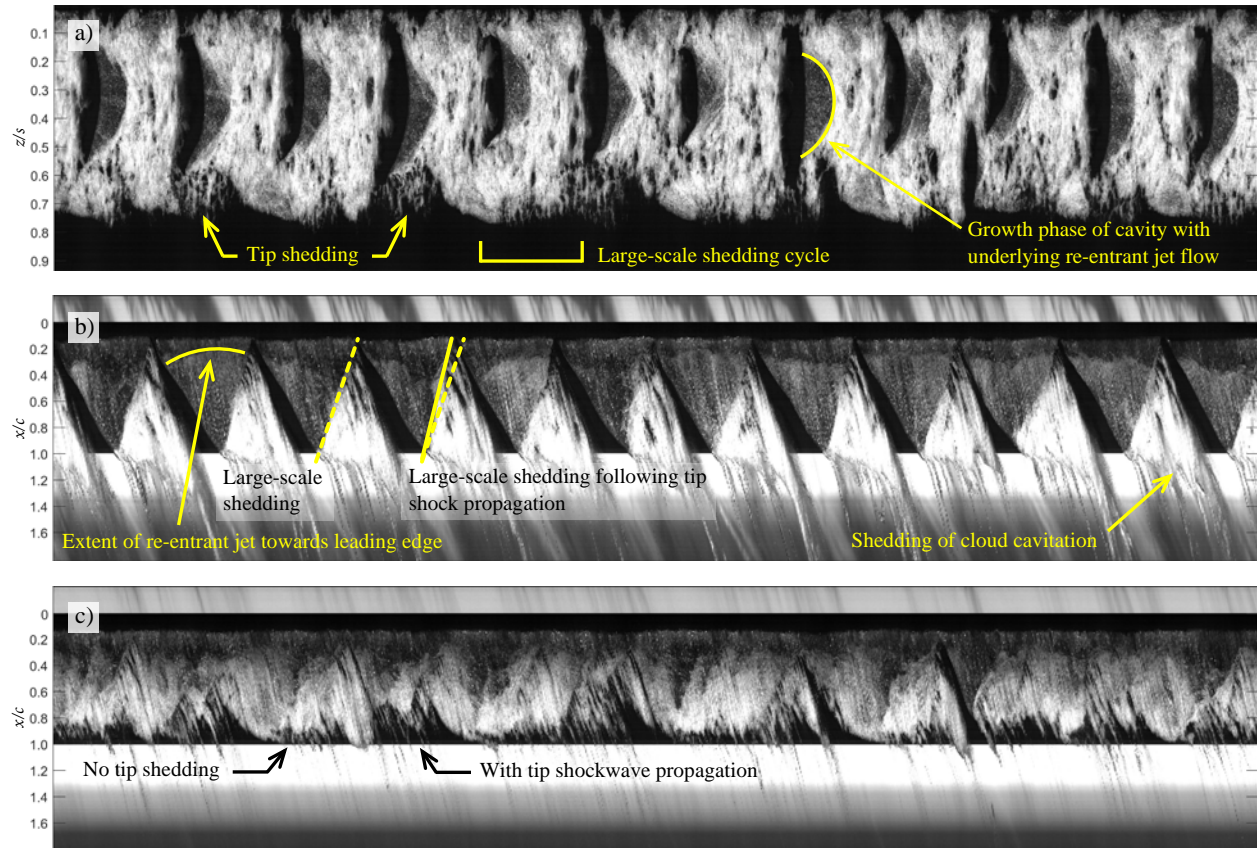


Figure 4: Space-time plots for the nuclei deplete case at  $\sigma = 0.55$ . Time progresses left-to-right, while position is the vertical dimension for the respective orientation: a) span-wise plot at 0.8c, b) chord-wise plot at 0.4s, and c) chord-wise plot at 0.7s.

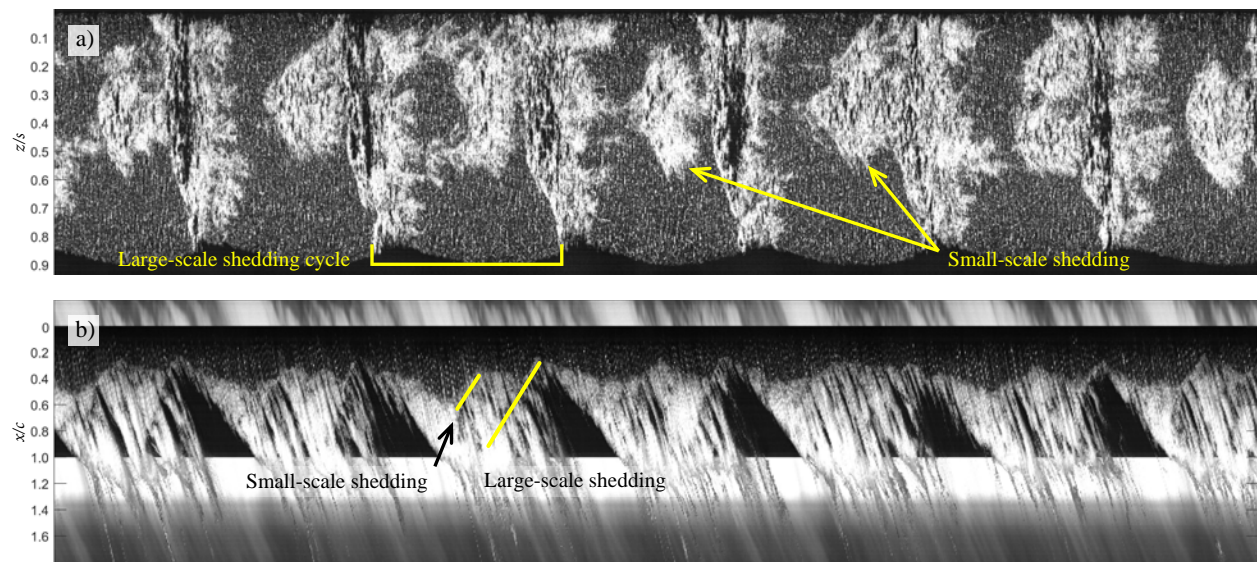


Figure 5: Space-time plots for the nuclei abundant case at  $\sigma = 0.55$ . Time progresses left-to-right, while position is the vertical dimension for the respective orientation: a) span-wise plot at 0.4c, and b) chord-wise plot at 0.4s.

## Conclusion

The spectral content of the body-normal force and the shedding dynamics of a cavitating NACA-0015 section hydrofoil has been studied to examine the effect of both cavitation number and freestream nuclei content. Tests were conducted at a constant Reynolds number over a range of cavitation numbers for test conditions both deplete of freestream nuclei, and with the injection of a high concentration of nuclei. Three distinct, yet coupled frequencies were observed in the nuclei deplete cases – the dominant frequency associated with large-scale shockwave induced cavity shedding at mid-span, the sub-harmonic with the alternating strength of localized tip shedding, and the first harmonic at twice the dominant mode frequency was associated with small-scale shedding activity at both root and tip. The frequencies were found to decrease with cavitation number over the narrow range tested. The presence of abundant freestream nuclei was found to alter the hydrofoil response and shedding characteristics. Two distinct frequencies were observed in the latter case, the dominant low-frequency mode associated with large-scale full-span cavity shedding. This dominant mode was observed at approximately half the frequency of the corresponding nuclei deplete mode in all cases. The higher frequency mode was due to an initial, weaker shock propagation centred at mid-span that resulted in only localized cavity condensation in between the passage of the large-scale shedding events.

## Acknowledgements

This project was supported by the Defence Science and Technology Group (Mr. Brendon Anderson and Dr. David Clarke), the University of Tasmania, and the US Office of Naval Research (Dr. Ki-Han Kim, Program Officer) and ONR Global (Dr. Woei-Min Lin) through NICOP S&T Grant no. N62909-15-1-2019.

## References

- [1] Kawakami, D. T., Fuji, A., Tsujimoto, Y., & Arndt, R. E. (2008). *An assessment of the influence of environmental factors on cavitation instabilities*. Journal of Fluids Engineering, 130(3).
- [2] Kjeldsen, M., Arndt, R. E., & Effertz, M. (2000). *Spectral characteristics of sheet/cloud cavitation*. Journal of Fluids Engineering, 122(3).
- [3] Ganesh, H., Wu, J., & Ceccio, S. L. (2016). *Investigation of cavity shedding dynamics on a NACA0015 hydrofoil using time resolved x-ray densitometry*. In 31st Symposium on Naval Hydrodynamics.
- [4] Tan, D., Li, Y., Miorini, R., Vagnoni, E., Wilkes, I., & Katz, J. (2014). *Role of large scale cavitating vortical structures in the rotor passage of an axial waterjet pump in performance breakdown*. In 30th Symposium on Naval Hydrodynamics.
- [5] Gnanaskandan, A., & Mahesh, K. (2016). *Large Eddy Simulation of the transition from sheet to cloud cavitation over a wedge*. International Journal of Multiphase Flow, 83.
- [6] Barbaca, L., Pearce, B. W., & Brandner, P. A. (2017). *Experimental study of ventilated cavity flow over a 3-D wall-mounted fence*. International Journal of Multiphase Flow, 97.
- [7] Ceccio, S., & Brennen, C. (1992). *Dynamics of attached cavities on bodies of revolution*. Journal of Fluids Engineering, 114(1).
- [8] Brandner, P. A., Walker, G. J., Niekamp, P. N., & Anderson, B. (2010). *An experimental investigation of cloud cavitation about a sphere*. Journal of Fluid Mechanics, 656.
- [9] Ganesh, H., Mäkiharju, S. A., & Ceccio, S. L. (2016). *Bubbly shock propagation as a mechanism for sheet-to-cloud transition of partial cavities*. Journal of Fluid Mechanics, 802.
- [10] de Graaf, K. L., Brandner, P. A., & Pearce, B. W. (2017). *Spectral content of cloud cavitation about a sphere*. Journal of Fluid Mechanics, 812.
- [11] Laberteaux, K. R., & Ceccio, S. L. (2001). *Partial cavity flows. Part 2. Cavities forming on test objects with spanwise variation*. Journal of Fluid Mechanics, 431.
- [12] Gindroz, B., & Billet, M. L. (1998). *Influence of the nuclei on the cavitation inception for different types of cavitation on ship propellers*. Journal of fluids engineering, 120(1).
- [13] de Graaf, K., Pearce, B., & Brandner, P. (2016). *The influence of nucleation on cloud cavitation about a sphere*. In 16th International Symposium on Transport Phenomena and Dynamics of Rotating Machinery (ISROMAC 2016).
- [14] Brandner, P. A., Lecoffre, Y., & Walker, G. J. (2007). *Design considerations in the development of a modern cavitation tunnel*. In 16th Australasian Fluid Mechanics Conference.
- [15] Venning, J. A., Khoo, M. T., Pearce, B. W., & Brandner, P. A. (2018). *Background nuclei measurements and implications for cavitation inception in hydrodynamic test facilities*. Under consideration for publishing in Experiments in Fluids.
- [16] Giosio, D., Pearce, B. W., & Brandner, P. A. (2016). *Influence of Pressure on Microbubble Production Rate in a Confined Turbulent Jet*. In 20th Australasian Fluid Mechanics Conference.
- [17] Venning, J., Smith, S., Brandner, P., Giosio, D., & Pearce, B. (2017). *The influence of nuclei content on cloud cavitation about a hydrofoil*. In 17th International Symposium on Transport Phenomena and Dynamics of Rotating Machinery (ISROMAC 2017).